Short-term extreme ice loads prediction and fatigue damage evaluation for an icebreaker

Wei Chai[a]*, Bernt J. Leira[a], Arvid Naess[b,c]

[a]*Department of Marine Technology, Norwegian University of Science and Technology, Trondheim, Norway;*

[b]*Centre for Ships and Ocean Structures, Norwegian University of Science and Technology, Trondheim, Norway;*

[c]*Department of Mathematical Sciences, Norwegian University of Science and Technology, Trondheim, Norway.*

Abstract: In this paper, the short-term extreme value statistics of the ice loads acting on ship hull and the fatigue damage due to ice loads actions are studied. Due to the stochastic nature of the ice-induced loads and randomness of the ice thickness, probabilistic methods and models are applied in order to find some correlations between the ice-induced loads statistics and the prevailing ice conditions. For the extreme value prediction, the ACER (average conditional exceedance rate) method is applied to approximate the exact extreme value distribution. The short-term fatigue damage is estimated based on the S-N curve approach. Furthermore, probabilistic models, such as the Weibull distribution and the three-parameter exponential distribution are applied to approximate the distribution of the stress ranges due to ice loads actions and the performance of the fatigue damage evaluation based on probabilistic distribution functions of the stress ranges is studied.

Keywords: Extreme ice loads; fatigue damage; ice thickness; probabilistic methods

1. Introduction

Increased activities in Arctic regions promote the requirement of ice class vessels and offshore structures. For ships and offshore structures subjected to wave loads and/or wind loads, extreme structural response analysis and fatigue damage evaluation have received a great attention in recent years (Cheng et al. 2017, Leira 2016, Naess and Moan 2012, Nejad et al. 2014). However, due to the complexity of the ship-ice interaction process and limited knowledge of the prevailing ice conditions, studies with respect to extreme ice

loads and fatigue damage of ship structures due to ice loads actions are still under development.

Former studies based on the full-scale measurements have demonstrated that ice-induced loads are stochastic, even though such ship-ice interaction process is governed by deterministic laws of mechanics (Leira et al. 2009, Lensu 2002). This random process depends on the variation of the prevailing ice conditions, the ship hull geometry and also the ship speed, etc. In fact, full-scale field experiments in the ice-covered regions with the information of ice-induced loads, prevailing ice conditions, operation situations, and engine data have been recommended as the most reliable method to validate theoretical models as well as for study the ice loads statistics and ice-induced structural response (ISSC 2015).

Ice thickness is assumed to be the most representative parameter for the severity of the ice conditions (Bergström et al. 2017). The ice thickness along the expedition route of the full-scale field experiment can be regarded as a random process with respect to the time space. Unfortunately, due to the stochastic nature of ice loads and ice thickness, it is a challenge to establish a link between the prevailing ice conditions and the ice-induced loads. Long-term data obtained over a number of years can provide such linkage, however, long-term measurements have been performed only in Baltic and Antarctic waters (Kujula 1994). In this work, the records of ice loads and ice thickness are collected by short-term full-scale measurement in the sea area of Svalbard islands. The aim of current work is to find some correlations between the ice thickness and the ice-induced loads statistics, such as the extreme value statistics and the fatigue damage due to ice loads actions. The extreme value statistics of ice loads and the fatigue damage are directly related to the ultimate limit states (ULS) and the fatigue limit states (FLS) of the vessel,

respectively (Naess and Moan 2012). Therefore, current study could promote the knowledge with respect to reliability-based design and operation of ice-capable vessels.

As for the extreme ice loads prediction, earlier studies have applied different probability distributions to fit the measured short-term ice load peaks (Kotilainen et al. 2017). This method is known as the peak amplitude approach and the distributions are usually the exponential distribution (Jordaan et al. 1993), log-normal distribution (Kujala and Vuorio 1986, Kujula 1994), Weibull distribution (Suominen and Kujala 2010) and also the three-parameter exponential distribution (Suyuthi et al. 2014). It should be noted that the peak amplitude method requires that all the variables (i.e. the ice load peaks) are stationary and independent. However, the stationary requirement can be satisfied only for some ideal cases. Nonstationary conditions are very common even for short-term measurements. In addition, dependence of neighbouring peaks is a common phenomenon for the ice loads and such effects will influence the performance of the peak amplitude method. Furthermore, by fitting the empirical cumulative distribution, the asymptotic method based on the Gumbel distribution can also be applied to estimate the extreme value (Lensu 2002). But the main weakness lies in the fact that the performance of the asymptotic method depends on the observed data and we cannot know to what extent it is applicable for the observed data in advance (Næss and Gaidai 2009).

In this work, a novel method, namely the ACER (average conditional exceedance rate) method, is introduced for prediction of extreme value statistics of ice loads. In this method, a sequence of nonparametric functions, i.e. the ACER functions with different orders, are constructed and applied in order to approximate the exact extreme value distribution. The empirical ACER functions can be calculated from the measured data and then an optimization procedure based on an extrapolation scheme and an assumed tail behaviour of the extreme value distribution is applied to provide a reasonable

estimation of the extreme ice loads in the far tail region. Moreover, construction of the ACER functions is available for both the stationary and non-stationary data sets. The derivation of the ACER functions and the principle of the optimization procedure are presented in Appendix in Ref. Chai et al. (2017) and Section 3 of current work, respectively. In addition to current study, the ACER method has been well benchmarked against existing conventional methods and applied for predicting the extreme ship roll response at seas (Gaidai et al. 2016), and the extreme wind speed (Karpa and Naess 2013), etc.

In addition to the extreme ice loads statistics, fatigue damage caused by cycle ice loading could also be an important issue for ice class ship navigating in severe ice regions (Suyuthi et al. 2013a, Zhang et al. 2011). Generally, fatigue damage evaluation are based on the S-N data in association with the Palmgren-Miner law of damage accumulation (Guedes Soares and Moan 1991). In this work, when the short-term time series of ice-induced stress ranges are available, fatigue damage of ship hull can be directly estimated by summing the fatigue damages of all stress cycles according to the linear Palmgren-Miner cumulative rule. On the other hand, fatigue damage can also be estimated by probabilistic manners when the distributions of the stress ranges are known. This method has been widely used for predicting the fatigue life of ships and offshore structures at the design stage (Nejad, Gao and Moan 2014, Zhang, Bridges and Tong 2011). However, fatigue life predictions are usually based on the long-term distribution of the stress ranges which is difficult to obtain by full-scale measurements. Nevertheless, it is still meaningful to investigate the feasibility of the (short-term) fatigue damage evaluation based on probabilistic manners. In this work, the Weibull and the three-parameter exponential distribution models are applied to approximate the distribution of the ice-induced stress ranges and their feasibility for fatigue damage evaluation is studied.

The paper is organized as follows. The full-scale measurement with information of ice loads, ice thickness and expedition route is described in section 2. The principle of the ACER method is illustrated in section 3 and the results of extreme ice loads prediction are presented in this section. Probabilistic models and results of fatigue damage due to ice loads actions are shown in section 4. The correlation between the prevailing ice conditions and the ice loads statistics are discussed in sections 3 and 4.

2. Measured ice thickness and ice loads

In this work, the full-scale measurement was conducted onboard the Norwegian coastguard vessel KV Svalbard. The expedition was performed in the sea area of Svalbard islands for two weeks in March 2007 (see Fig. 1) and the information with respect to the ice conditions, the navigation data (e.g. ship speed, propulsion power) as well as the records of ice-induced loads on ship hull along the expedition route were recorded by an Ice Load Monitoring system. Ice thickness along the expedition route was measured by means of an electromagnetic tool, which was mounted on a wooden beam protruded ahead of the vessel. Descriptions with respect to the principle of ice thickness measuring device can be found in Leira, Børsheim, Espeland and Amdahl (2009). In addition, the ice conditions shown in Fig. 1 were measured from seven consecutive days only, i.e. from 22nd to 28th, March (Suyuthi et al. 2012).

When a ship moves in the ice-covered regions, the recorded thickness of sea ice can be considered as a random process. In order to find a correlation between the prevailing ice conditions and the ice-induced loads statistics, two 3-hour data sets collected by the Ice Load Monitoring system are selected. The first short-term condition denoted as case a and started from 18:30 to 21:30 on March 26th, 2007 and the second 3-hour condition is referred to as case b and started from 09:00 to 12:00 on March 28th, 2007. Fig. 2 shows the distributions of measured thickness during the two short-term cases and Fig. 3

presents two examples of ice thickness recorded along the expedition route as a variable with respect to time *t*.

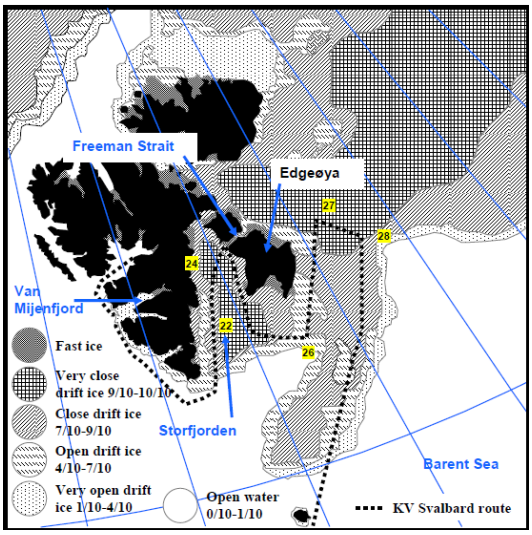

Figure 1. Expedition route of KV Svalbard in the sea area of Svalbard islands in March 2007, number 22, 24, …, 28 represent the dates and position of the vessel in the morning of each day (Suyuthi et al. 2013b).

There was no observations of multi-year ice floes along the expedition route and the prevailing ice conditions are mostly first-year (Pfaffling 2007). In the field of probability theory, stationarity of the ice conditions is required for developing probabilistic models for the ice thickness as well as for the ice-induced load process. However, such stationary condition can only be encountered in some ideal conditions, such as the level ice field. Non-stationary cases of the ice conditions and the ice-induced load process are very common during the full-scale measurements, even for short-term cases. For example, it is seen in Fig. 3 that both of the time series are non-stationary since the mean values and the standard deviations of the ice thickness are time-dependent. Moreover, it is seen in Fig. 2, for the two short-term cases, the ice condition for case a is more serious than case b. Specifically, the thin first-year ice (0.3-0.7 m thick) makes up a larger percentage in case b, while case a has more contributions from the medium thick first-year ice (0.7-1.2 m thick) and thick first-year ice (over 1.2 m thick).

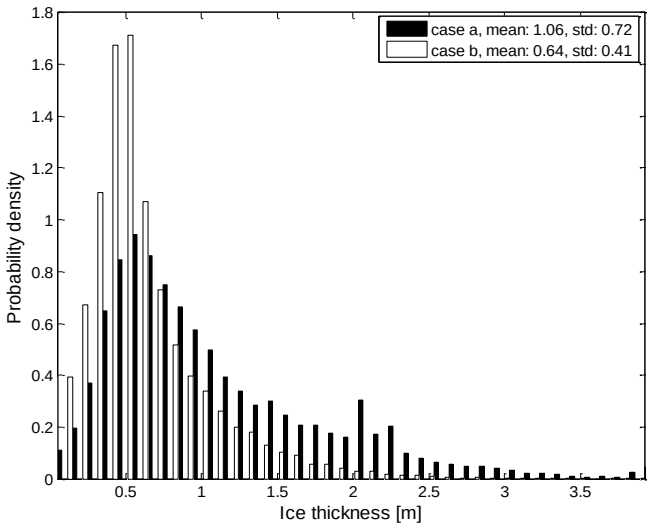

Figure 2. Histograms (probability density) of the recorded ice thickness for case a (18:30-21:30, March 26th, 2007) and case b (09:00-12:00, March 28th, 2007).

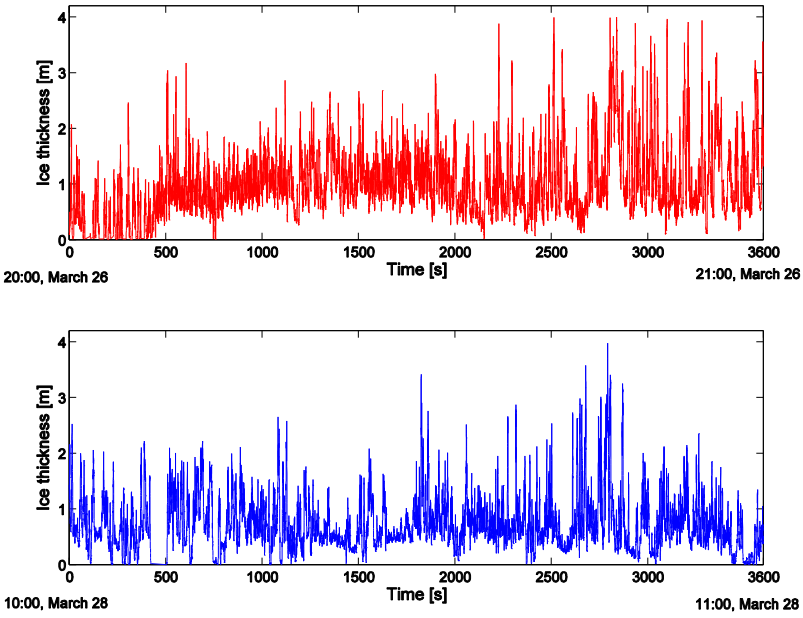

Figure 3. Time series of observed ice thickness, upper: 1 hour time series in case a, lower: 1 hour time series in case b.

The local ice loads, i.e. loads induced by the ice on the ship's shell and acting on the transverse frames during the ice-breaking process are considered in this work. Within the Ice Load Monitoring system, the fiber optic strain sensors were instrumented in order to record the local ice loads in the bow region (L1-L4 in Fig. 4) and the bow intermediate region (L5-L8) where the loading levels are significantly higher than other regions

(Nyseth 2006). The arrangement of the sensors is shown in Fig. 4 and L1, …, L8 represent the location numbers. The measured shear strain is converted into shear stress, and then the total shear force can be obtained by integrating the (pre-assumed) shear stress distribution over the cross section of the frame. Therefore, the local ice load can be taken as the difference between the shear forces at the upper and lower parts of the frame. The load on a transverse frame has a unit [kN], but for practical applications it is usually treated as a line loads by dividing the load by the frame spacing of the transverse frame and then the new unit is [kN/m]. Furthermore, the ice load measurements are associated with the specific site shown in Fig. 1 and the measured ice loads cannot be applied to other sites.

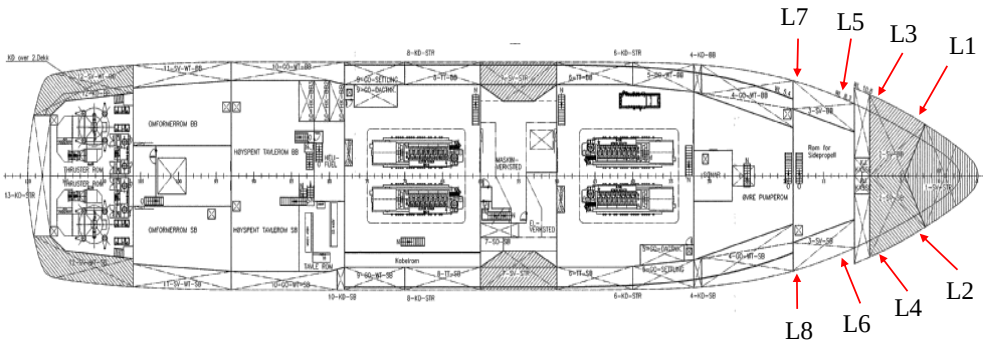

Figure 4. Locations of strain sensors.

The measured ice-induced loads looks like a sequence of impulses with sharp peaks which can be explained by the ice-breaking process (Kotilainen, Vanhatalo, Suominen and Kujala 2017). The sharp peaks indicate that the accumulated crushing force during the ship-ice interaction process is high enough to initiate bending failure of the ice features. Such impulses is repeated as the ice-breaking process continues. The peak values of the loads during the ice-breaking process is referred to as the ice load peaks which are used for relevant analysis in the following work.

It is known that the ice load peaks depend on the prevailing ice conditions, ship hull geometry and the ship speed. However, such relationship is not straightforward. Generally, the ice-induced loads increase with the severity of the ice conditions and increased ship speed. But Leira, Børsheim, Espeland and Amdahl (2009) also suggested that for some small ships or for some specific cases, ship speed was reduced considerably when the vessel experience a high resistance from the ice sheet. That means thick ice does not always correspond to large ice load peaks and ice loads can also increase as ship speed decreases. Nevertheless, much severer ice conditions imply that it is more probable to generate large ice loads from a probabilistic view.

In this work, the correlation between the prevailing ice conditions and the ice-induced loads statistics is studied and the influence of the ship speed is not considered for simplicity. Fig. 5 shows two examples of the ice load peaks recorded by the strain sensors located at L6 for the two short-term conditions correspond to different ice conditions. Table 1 presents the number of ice load peaks, the mean values, standard deviations and the coefficients of variation (cov) of the recorded ice load peaks at different locations for the two short-term conditions. It is seen in Table 1 that there is no direct correlation between the ice thickness and the number of ice load peaks. Also, there is no significant variations of the mean values at different locations as well as for different short-term conditions. However, it is seen that case a (i.e. the short-term case with heavier ice conditions) corresponds to larger values of the standard deviations and cov for the ice load peaks which indicate that the peak loads have a wider range of values, especially in the region beyond the mean values. Based on the ice load peaks collected at different locations, the short-term extreme value statistics of the ice loads and the fatigue damage due to ice loads action are studied in Sections 3 and 4, respectively.

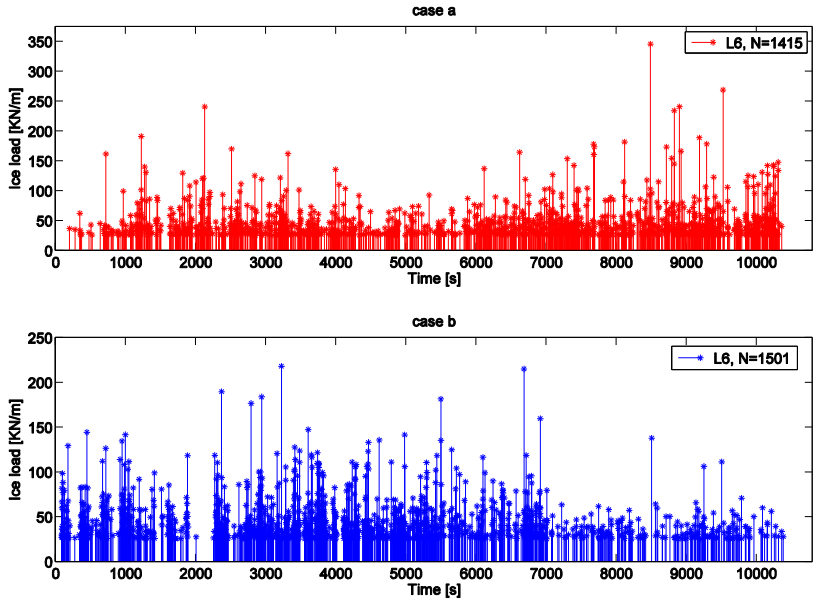

Figure 5. Time series of ice load peaks recorded at L6 for two short-term conditions, N represents number of ice load peaks

Table 1. Numbers (N) of ice load peaks for two short-term cases and the associated mean values (kN/m), standard deviations (kN/m) and coefficients of variation (cov).

Location	case a				case b			
	N	mean	std	cov	N	mean	std	cov
L1	573	45.40	22.94	0.51	572	43.85	17.95	0.41
L2	513	47.08	23.70	0.50	544	44.94	19.65	0.44
L3	516	48.07	28.27	0.59	470	45.73	21.15	0.46
L4	604	47.62	24.10	0.51	652	45.67	21.00	0.46
L5	1147	44.10	24.69	0.56	1067	43.22	22.47	0.52
L6	1415	46.11	28.29	0.61	1501	44.74	23.58	0.53
L7	1065	46.13	25.80	0.56	1216	45.05	23.42	0.52
L8	580	43.90	23.39	0.53	701	41.11	19.01	0.46

3. Extreme ice loads prediction

3.1 ACER method

The aim of this Section is to determine the extreme value distribution of ice load peaks. Consider the ice load peaks as a stochastic process $X(t)$, which has been observed over the time period $[0, T]$. Assume that the ice load peak values $X_1, X_2, \ldots, X_N$ are allocated to the discrete times $t_1, t_2, \ldots, t_N$ in the time interval $[0, T]$ and N is the number

of observed ice load peaks. The extreme value among the N outcomes of the stochastic process $X(t)$ is defined as: $M_N = \max\{X_1,\ldots,X_N\}$ and then the extreme value distribution is expressed as:

$$P(\eta) = \mathrm{Prob}(M_N \le \eta) = \mathrm{Prob}(X_1 \le \eta,\ldots, X_N \le \eta) \quad (1)$$

The time series of the ice load peaks for the selected short-term conditions are clearly non-stationary since the ice thickness is non-stationary. The ACER method, which can utilize the full nonstationary data set, is applied in order to assess the extreme value statistics of the ice load peaks. The main principle of the method lies in the fact that a sequence of nonparametric functions based on the ACER functions with different orders, are constructed to approximated the exact extreme value distribution expressed as Equation (1).

The derivation of the sequence of nonparametric functions, $P_k(\eta)$ for different order k and the associated ACER functions ε_k for order k are given as Appendix in Ref. (Chai, Leira and Naess 2017). With the time series of ice load peaks measured at different locations, the extreme value distribution is approximated as:

$$\mathrm{Prob}(M_N \le \eta) \approx P_k(\eta) \approx \exp(-(N-k+1)\hat{\varepsilon}_k(\eta)) \quad (2)$$

where $\hat{\varepsilon}_k$ is the empirical ACER function of order k, which can be obtained by applying the existed time series.

In order to predict the extreme value distribution when the level η is sufficiently large, an extrapolation scheme is applied. This technique is based on the observations that for ships and offshore structures being considered, the mean upcrossing rate and the ACER functions are in general highly in a specific way in the tail region. For a wide range of dynamical systems, the tail of the ACER functions (e.g. $\eta \ge \eta_0$) behaves similarly to $\exp\{-a(\eta-b)^c\}$, where $a > 0$, $b \le \eta_0$ and $c > 0$ are suitable constants. The empirical ACER function is therefore assumed to be in the form of:

$$\hat{\varepsilon}_k(\eta) \approx q_k \exp(-a_k(\eta - b_k)^{c_k}), \eta \geq \eta_0 \quad (3)$$

where a_k, b_k, c_k and q_k are suitable constants which are dependent on the number of order k.

Generally, under the aforementioned assumptions for the tail region of the ACER functions, plotting $\log|\log(\hat{\varepsilon}_k(\eta)/q_k)|$ verus $\log(\eta\text{-}b_k)$ would give an almost perfect linear tail behavior. In this work, the more robust Levenberg-Marquardt least squares optimization method is used to determine the optimal values for a_k, b_k, c_k and q_k. Details of this method can refer to Naess and Moan (2012) and Chai et al. (2016).

3.2 Extreme ice loads

In this part, the ACER method described above is applied to predict the extreme ice loads. Firstly, time series of ice load peaks collected at L6 for the two short-term cases (shown in Fig. 5) are selected as examples. Then, empirical ACER functions, $\hat{\varepsilon}_k$, for different orders of k can be obtained and Fig. 6 presents the ACER functions versus different ice load peaks for the two cases. It is seen from Fig. 6 that for the lower range of ice load values, there is an effect of dependence between the data points. However, this effect does vanish in the tail, indicating that all the ACER functions will coalesce in the deep tail. This allows the use of the first ACER function $\hat{\varepsilon}_1(\eta)$ for extrapolation purposes. This is advantageous since the first ACER function is the one which is most accurately estimated because more data are available for its estimation, thereby enhancing the precision.

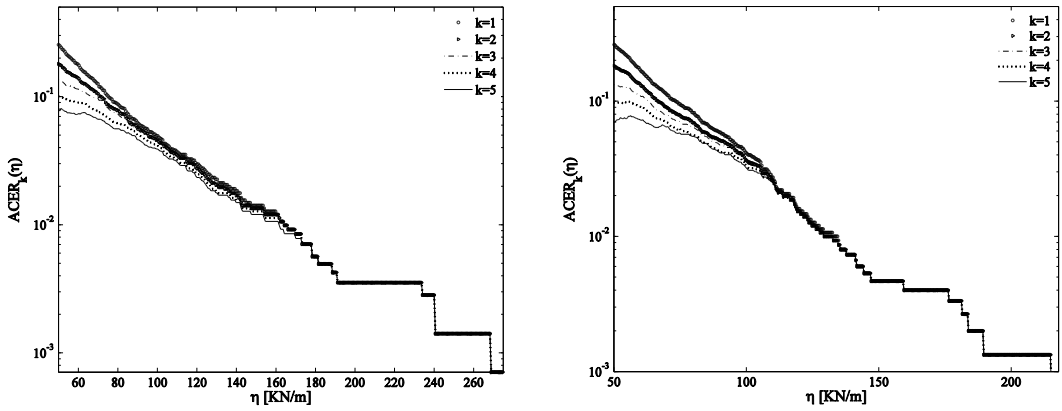

case *a* case *b*

Figure 6. ACER functions with different order *k* for the ice load peaks collect at location L6 for two short-term cases

The target exceedance probability for each 3-hour short-term case is determined to be 0.1, i.e. 1- Prob($M_N \leq \eta$) = 0.1. Then, the 90% fractile value for each short-term case can be estimated by Equation (2). Based on the $ACER_1$ functions, $\hat{\varepsilon}_1(\eta)$, and the extrapolation scheme, the target extreme ice loads at L6 for the two short-term cases can be estimated. Figs. 7 and 8 illustrate estimations of the target extreme values by application of the ACER method. Moreover, the predicted ACER functions in the far tail regions and the fitted 95% confidence intervals are also plotted in these two figures.

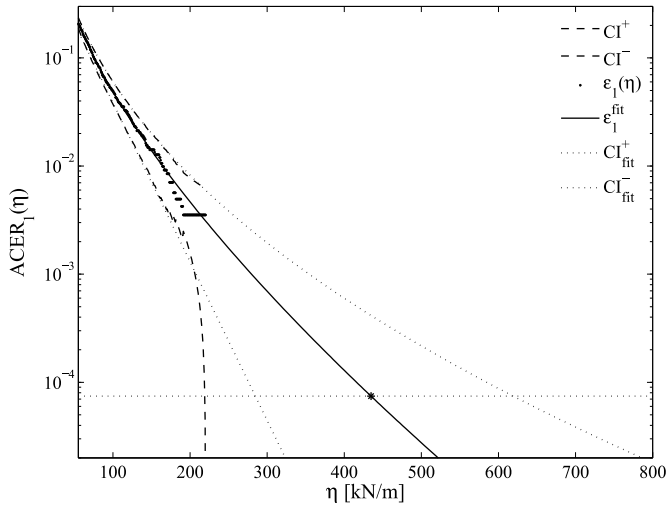

Figure 7. Extreme ice load prediction based on the $ACER_1$ function for L6, case a, a_1 = 0.1483, b_1 = 37.131, c_1 = 0.686, q_1 = 0.621, η_0 = 55.0.

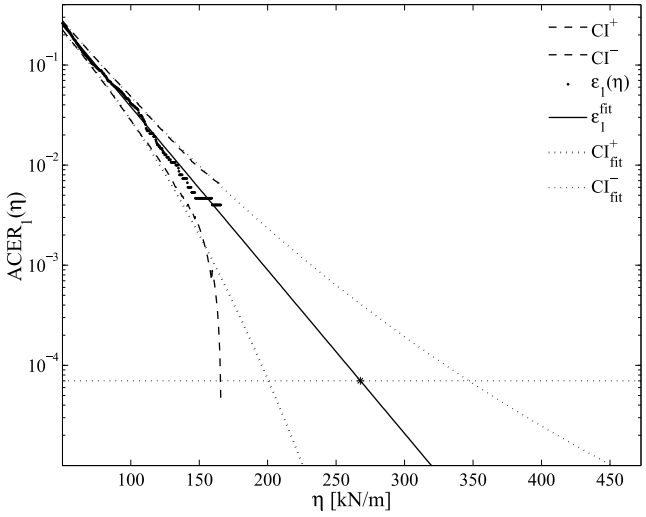

Figure 8. Extreme ice load prediction based on the $ACER_1$ function for L6, case b, a_1 = 0.0376, b_1 = 44.763, c_1 = 1.0, q_1 = 0.305, η_0 = 50.0.

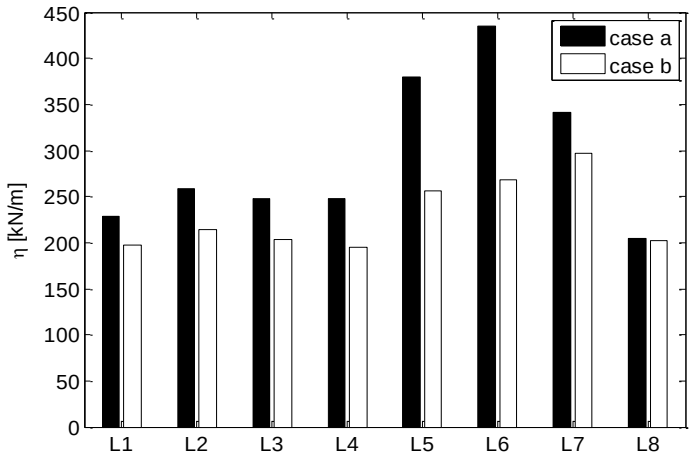

Figure 9. 90% fractile values at different locations for the two short-term cases, estimated by the ACER method.

Similarly, the 90% fractile values at the other locations can also be estimated by the ACER method. In these cases, the ACER functions with the order k = 1 are used and the target extreme values at different locations for each short-term case are shown in Fig. 9. It is observed that the extreme ice loads in the bow intermediate region (i.e. L5-L8 in Fig. 4) are much severer than the bow area (L1-L4) for each 3-hour case, and such difference is more noticeable for case a, which corresponds to a heavier ice condition. Moreover, for

all locations except L8, the extreme values during the short-term case a are higher than the values for case b with weaker ice conditions.

The bow area is the first region to contact and break the ice features during the ice-breaking process, but the ship-ice interaction process occurs more frequently in the bow intermediate region for each short-term case, since more ice load peaks (see Table 1) were collected in locations L5 - L8. It is seen in Fig.9 and Table 1 that there is no correlation between the mean value of the ice load peaks and the extreme values. From the ACER method given as Eqs. 2 and 3, the target extreme value depends on the number of the observed ice load peaks N as well as on the ACER functions in the tail region (e.g. $\eta \geq \eta_0$).

It is also seen in Table 1 that the numbers of ice load peaks collected at the same location for different short-term cases are very close, but there is a clear discrepancy between the corresponding extreme values at some locations. This could be explained by the fact that case a has more contributions from the medium and thick first year ice, which are more probable to generate large values of the ice loads peaks. On the other hand, case b has larger percentages of the thin first year ice and the peak ice loads have a narrower distribution and less number of data in the tail region, which corresponds to lower extreme values of ice loads.

4. Fatigue damage evaluation

4.1 Fatigue prediction methods

The fatigue damage during a particular short-term condition can be evaluated by application of the linear Palmgren-Miner cumulative rule, which is given as the following expression:

$$D = \sum_{i=1}^{w} \frac{n_i}{N_i} \tag{4}$$

where D is the fatigue damage during the short-term condition. It is assumed that the stress cycles induced by the ice loads can be divided into w different ranges S_i $(1 \le i \le w)$, and each range contributes $n_i(S_i)$ cycles. $N_i(S_i)$ is the number of stress cycles to failure for the stress range S_i, which is given by the S-N curve:

$$N_i = K \cdot S_i^{-m} \tag{5}$$

in which K and m can be obtained from the design S-N curves. By inserting Eq. 5 into Eq. 4, the fatigue damage for each short-term condition can be obtained:

$$D = \frac{1}{K} \sum_{i=1}^{w} n_i S_i^m = \frac{N_T}{K} \sum_{i=1}^{w} S_i^m f_S(S_i) \Delta S \tag{6}$$

where N_T is the total number of stress cycles during the short-term period [0, T], f_S is the distribution of stress ranges and ΔS represents the width of the stress range.

It is seen in Eq. 6 that the total number of stress cycles and the distribution of stress ranges should be determined in order to evaluate the fatigue damage. Due to the nature of ice-induce loads, the related stress process also behaves as a sequence of impulses with sharp peaks (Hwang et al. 2016, Suyuthi, Leira and Riska 2013a). Therefore, for the cases of fatigue damage caused by the ice loads actions, the stress cycles (or stress ranges) can be replaced by the stress amplitudes and the total number of stress cycles is equal to the number of stress peaks. Assume that there is a linear transformation between the ice-induced load process and the ice-induced stress process, the transformation is written as:

$$S(t) = \gamma X(t) \tag{7}$$

where $X(t)$ is the ice load peaks mentioned in Section 3 and $S(t)$ is the corresponding stress amplitudes and it also represents the stress range in the following study. γ is the

transformation factor, which can be determined by using structural beam theory or by a proper structural analysis (Zhang, Bridges and Tong 2011).

In addition to the above direct calculations, fatigue damage can also be estimated by applying the fitted distribution of the stress range and then Eq. 6 can be approximated as:

$$D \approx \frac{N_T}{K}\int_0^{\infty} S^m f_S(S)dS \tag{8}$$

According to the former studies, the measured ice load peaks can be fitted by different probability distributions, such as the log-normal, Weibull and three-parameter distributions, etc. Since the ice-induced stress process is assumed to be related to the ice-induced loads by an linear transformation given as Eq. 7, $S(t)$ can also be fitted by probabilistic models. In this work, the Weibull distribution (Rahman et al. 2015) and the three-parameter exponential distribution (Suyuthi, Leira and Riska 2014) are applied in order to approximate the process $S(t)$, which are written as:

$$f_{S_1}(S_1) = \frac{h}{p}\left(S_1/p\right)^{h-1}\exp\left\{-\left(S_1/p\right)^h\right\} \tag{9}$$

and

$$f_{S_1}(S_1) = \lambda e_1 \exp(-e_1 S_1) + (1-\lambda)e_2 \exp(-e_2 S_1) \tag{10}$$

, respectively. h and p are the shape and scale parameters for the Weibull distribution. λ, e_1 and e_2 are parameters for the three-parameter exponential distribution. For the Weibull distribution and the three-parameter exponential distribution, the parameters h, p and λ, e_1, e_2 are estimated by subtracting the lower threshold δ, i.e. $S_1 = S - \delta$, since the distribution f_{S_1} given by Eqs. 9 and 10 should be 0 when $S_1 = 0$. The effect of the lower threshold δ must be included in the fatigue damage evaluation. Correspondingly, the fatigue damage in Eq. 8 will be modified as:

$$D \approx \frac{N_T}{K}\int_{\delta}^{\infty} S^m f_S(S)dS = \frac{N_T}{K}\int_{\delta}^{\infty} S^m \frac{h}{p}\left((S-\delta)/p\right)^{h-1}\exp\left\{-\left((S-\delta)/p\right)^h\right\}dS \tag{11}$$

for the Weibull distribution. By introducing the transformation $\varphi = ((S\text{-}\delta)/p)^h$, we have

$$D \approx \frac{N_T}{K}\int_0^\infty (\delta + p\varphi^{\frac{1}{h}})^m \exp(-\varphi)d\varphi \tag{12}$$

Similarly, by introducing the transformations $\varphi_1 = e_1(S\text{-}\delta)$ and $\varphi_2 = e_2(S\text{-}\delta)$, the fatigue damage expressed by Eq. (10) is given as:

$$\begin{aligned} D &\approx \frac{N_T}{K}\int_\delta^\infty S^m \lambda e_1 \exp(-e_1(S-\delta)) + (1-\lambda)e_2 \exp(-e_2(S-\delta))dS \\ &= \frac{N_T}{K}\left[\lambda\int_0^\infty (\delta + \frac{\varphi_1}{e_1})^m \exp(-\varphi_1)d\varphi_1 + (1-\lambda)\int_0^\infty (\delta + \frac{\varphi_2}{e_2})^m \exp(-\varphi_2)d\varphi_2\right] \end{aligned} \tag{13}$$

When the parameter m is an integer, Binomial theorem and gamma function can be applied to given analytical values of Eqs. 12 and 13, otherwise numerical method should be introduced for the integration calculation. Furthermore, when considering a detailed structural component which involves stress concentration due to geometric imperfections, the stress concentration factor χ should be incorporated into the expression of the fatigue damage. Then the maximum stress amplitude (or hotspot stress range) S_χ should be applied instead of the nominal stress amplitude S given in Eqs. 6 and 7. The concentration factor χ is defined as (DNV 2014):

$$\chi = S_\chi / S \tag{14}$$

Correspondingly, the fatigue damage due to stress concentration, D_χ, based on direct calculation, is given as:

$$D_\chi = \frac{N_T}{K}\sum_{i=1}^{w} S_{\chi,i}^m f_{S_\chi}(S_{\chi,i})\Delta S_\chi \overset{f_{S_\chi}(S_{\chi,i})\Delta S_\chi = f_S(S_i)\Delta S}{=} \frac{N_T}{K}\sum_{i=1}^{w}(\chi S_i)^m f_S(S_i)\Delta S = \chi^m D \tag{15}$$

Similarly, the fatigue damage due to stress concentration, based on the probability distributions and derivations in Eqs. 11 and 13 are expressed as:

$$D_\chi \approx \frac{N_T}{K}\int_0^\infty (\delta + \chi p\varphi^{\frac{1}{h}})^m \exp(-\varphi)d\varphi \tag{16}$$

for the Weibull distribution and

$$D_{\chi} \approx \frac{N_T}{K}\left[\lambda\int_0^{\infty}(\delta+\frac{\chi\varphi_1}{e_1})^m \exp(-\varphi_1)d\varphi_1+(1-\lambda)\int_0^{\infty}(\delta+\frac{\chi\varphi_2}{e_2})^m \exp(-\varphi_2)d\varphi_2\right] \quad (17)$$

for the three-parameter exponential distribution.

4.2 Fatigue damage results

The fatigue damages due to ice loads actions are studied in this part. In the following study, the SN curve with $K = 10^{15.117}$ and $m = 4.0$ is selected (DNV 2014). The structural details has been described in Ref. Suyuthi, Leira and Riska (2013a), the transformation factor γ is 0.4708 and hot spot stress is used for fatigue evaluation with the stress concentration factor $\chi = 3.0$. Since the lower limit of the ice loads peaks is 25 kN/m, the lower threshold δ for the stress amplitude is 11.77 Mpa. According to the formula given by Eq. 15, the fatigue damages during the two short-term conditions can be calculated directly by application of the collected ice loads.

Fig. 10 presents the corresponding fatigue damages at different locations for the two short-term conditions. In each calculation, the number of stress ranges w is determined to be 60. Similar to the extreme values shown in Fig. 9, it is observed in Fig. 10 that for both of the short-term cases, fatigue damages in the bow intermediation region are generally severer than the damages in the bow area. Also, it is seen that for all of the locations, there is a noticeable discrepancies between the fatigue damages for different prevailing ice conditions.

In order to provide a more detailed study of the fatigue damage due to ice loads actions, a Table with different stress ranges and their contributions to the accumulated fatigue damage is introduced. The contribution is given as percentage which means the ratio between the fatigue damages due to a particular stress range and the overall damage D_{χ} provided by Eq. 15. In the following study, the ice load peaks collected at L6 for the two

different short-term cases are selected as the examples and relevant results for the contributions are shown in Table 2.

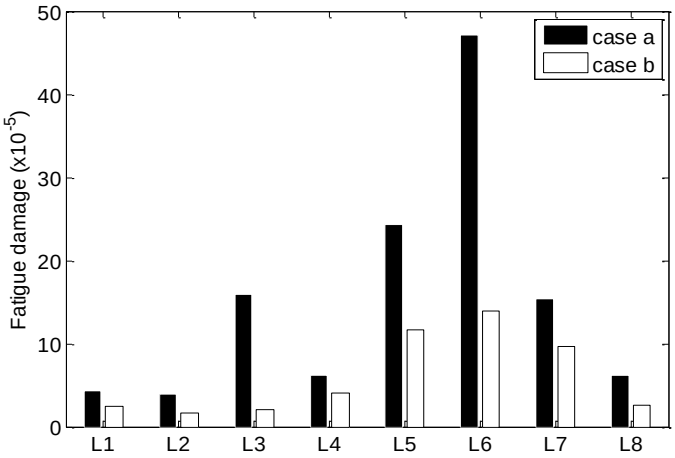

Figure 10. Fatigue damage at different locations for the two short-term cases, based on the collected records of ice load peaks.

Table 2. Number of stress ranges, accumulated fatigue damage and contributions to the overall fatigue damage based on the collected ice load peaks at L6 for two different short-term cases

case a				case b			
Stress range (Mpa)	n_i	Fatigue damage	Percentage (%)	Stress range (Mpa)	n_i	Fatigue damage	Percentage (%)
13.02-20.57	984	1.11E-5	2.36	12.53-17.07	789	3.24E-6	2.42
23.08-30.62	237	1.72E-5	3.66	18.58-23.12	333	5.75E-6	4.29
33.13-40.67	102	2.80E-5	5.95	24.64-29.18	163	8.00E-6	5.97
43.18-50.72	40	2.97E-5	6.31	30.69-35.23	80	8.59E-6	6.41
53.23-60.77	22	3.63E-5	7.72	36.75-41.29	46	9.71E-6	7.25
63.28-70.82	10	2.93E-5	6.22	42.80-47.34	31	1.18E-5	8.84
73.34-80.87	10	5.61E-5	11.91	48.85-53.40	28	1.77E-5	13.21
83.39-90.92	5	4.36E-5	9.26	54.91-59.45	14	1.38E-5	10.27
93.44-100.98	0	0.00E0	0.00	60.97-65.51	6	9.16E-5	6.83
103.49-111.03	1	2.36E-5	5.02	67.02-71.56	4	7.91E-6	5.90
113.54-121.08	2	5.17E-5	10.97	73.07-77.61	1	2.90E-6	2.16
123.59-131.13	1	3.93E-5	8.35	79.13-83.67	0	0.00E0	0.00
133.64-141.18	0	0.00E0	0.00	85.18-89.72	4	1.48E-5	11.05
143.69-151.23	0	0.00E0	0.00	91.24-95.78	0	0.00E0	0.00
153.75-161.28	1	1.05E-4	22.33	97.29-101.83	2	2.01E-5	15.03
Sum	1415	4.71E-4	100.00	Sum	1501	1.33E-4	100.00

According to mean values and standard deviations of ice load peaks given in Table 1 and relationship shown by Eq. 6, the mean values (u) and standard deviations (σ) for the stress amplitudes can be obtained. It is found in Table 2 that the stress ranges in the region with $S \geq u+3\sigma$ dominate the fatigue damage. In addition, it is seen in Eq. 15 that the contribution from each region of stress range is independent of the value of K and the concentration factor χ. The fatigue damage is proportional to S^m, and the stress ranges in the tail region are very important even though there is a very small number of stress ranges in this region.

Based on the above studies, the short-term fatigue damages shown in Fig. 10 are discussed in detail. It is seen in Table 1 and Fig. 10 that there is no relationship between the fatigue damage and the mean value of stress amplitudes. From Eq. 6 and observations above, the fatigue damage is directly related to the number and distribution of stress amplitudes, especially in the tail regions (e.g. $S \geq u+3\sigma$). The difference between the fatigue damages in the bow intermediation region and bow area is mainly caused by the number and the distribution of ice load peaks, especially in the large amplitude regions. Moreover, for different ice conditions, more serious ice condition means more probable to generate large values of stress ranges which play a dominant role for the overall fatigue damage. Therefore, the fatigue damages during the short-term a are significantly severer than the fatigue damages during the short-term condition b.

4.3 Fatigue damage based on probabilistic models

From the studies above, large values of stress ranges play an important role for the accumulated fatigue damage and then the assumptions about the type of probabilistic distribution functions for the stress ranges have a significant influence on the estimated fatigue damage. In this part, the probabilistic models, i.e. the Weibull and the three-

parameter exponential distribution model are applied to fit the distribution of the stress ranges and their performance for fatigue damage evaluation is investigated.

For the Weibull distribution model, the Weibull probability paper and the least square method are applied to calculate the scale and shape parameters. The parameters in the three-parameters exponential distribution are determined by the maximum likelihood approach (Suyuthi, Leira and Riska 2014). Figs. 11 and 12 present the fitting results of the two probabilistic models by applying the exponential probability paper. The empirical distributions (denoted as raw data) in these two Figs. are obtained by applying the ice load peaks collected at L6 during the two short-term conditions. Correspondingly, the probability densities of the of the two distribution models and the histograms of stress ranges are plotted in Figs 13 and 14. It is seen from Figs. 11 and 12 that both of the probabilistic models have satisfactory performance in the region $S < u+3\sigma$. However, in the tail region, such as $S \geq u+3\sigma$, discrepancies have been observed for both of the models.

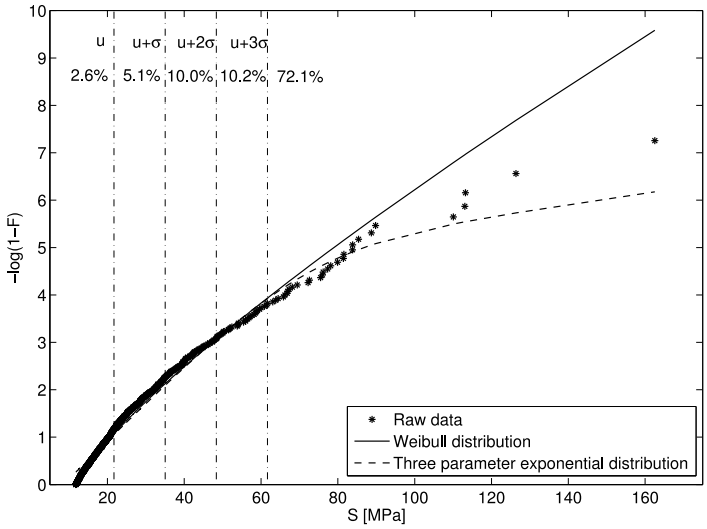

Figure 11. Exponential probability paper for the stress ranges *S*, based on the data collected at L6 for the short-term case a, the Weibull and the three-parameter exponential distribution.

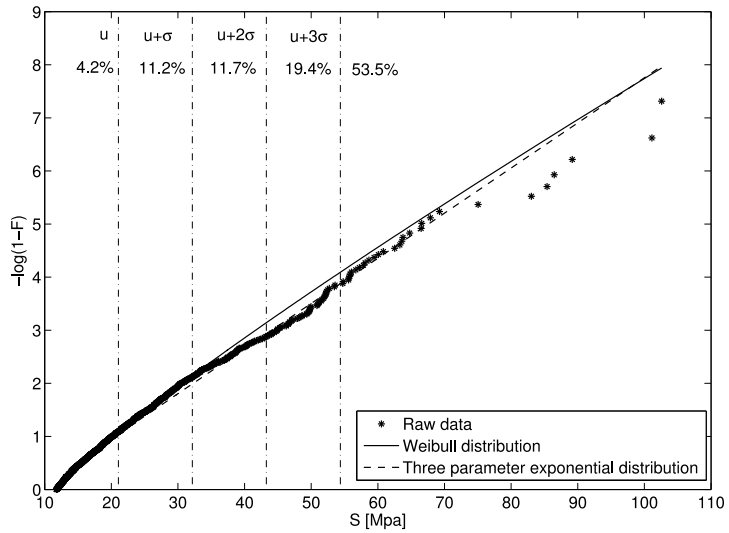

Figure 12. Exponential probability paper for the stress ranges *S*, based on the data collected at L6 for the short-term case b, the Weibull and the three-parameter exponential distribution.

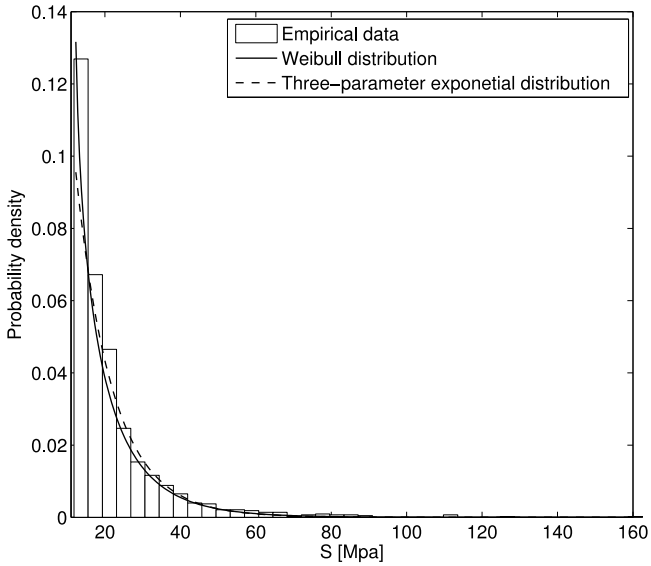

Figure 13. Distribution of the stress ranges S, based on the data collected at L6 for the short-term case a and fitted probability density functions of the Weibull and three-parameter exponential distributions.

The comparisons of the fatigue damage evaluated by direct calculation (i.e. Eq. 15) and the fatigue damage estimated by application of the probabilistic models are shown in Table 3. From the sensitive study given in Table 3, it is seen that the Weibull distribution leads to an underestimation of the fatigue damage for both of the short-term cases. The

performance of the three-parameter exponential distribution depends on specific conditions, i.e. it results in conservative approximation of the fatigue damage for some cases, and underestimate the damage for other cases.

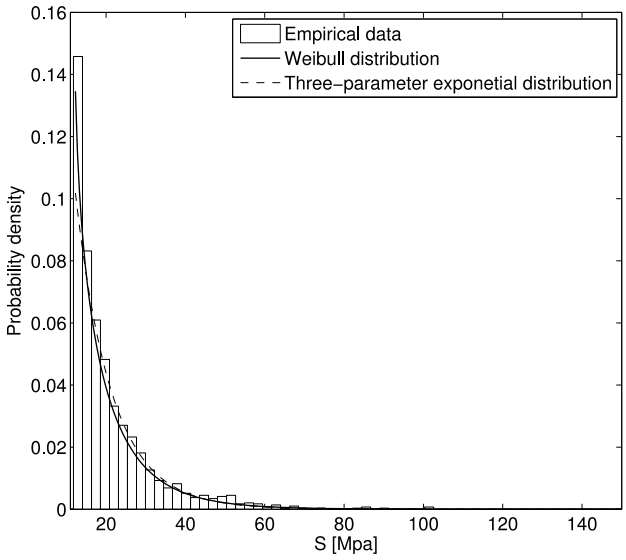

Figure 14. Distribution of the stress ranges S, based on the data collected at L6 for the short-term case b and fitted probability density functions of the Weibull and three-parameter exponential distributions.

Table 3. Comparisons of the fatigue damage calculated by Eq. 15 (D_δ) based on the data collected at L6 and the fatigue damages approximated by application of the probabilistic models (D_W : Weibull distribution, D_e: three-parameter exponential distribution).

Location	case a					case b				
	D_δ ($\times 10^{-5}$)	D_W ($\times 10^{-5}$)	D_W / D_δ	D_e ($\times 10^{-5}$)	D_e / D_δ	D_δ ($\times 10^{-5}$)	D_W ($\times 10^{-5}$)	D_W / D_δ	D_e ($\times 10^{-5}$)	D_e / D_δ
L1	4.36	1.61	0.37	1.67	0.38	2.42	0.61	0.25	5.79	2.39
L2	3.97	1.82	0.46	1.71	0.43	1.66	1.15	0.69	0.92	0.55
L3	15.87	1.51	0.10	43.8	2.76	2.03	0.82	0.40	1.07	0.53
L4	6.22	3.26	0.52	16.2	2.60	4.05	1.70	0.42	9.29	2.29
L5	24.31	2.21	0.09	69.3	2.85	11.68	2.09	0.18	30.1	2.58
L6	47.13	8.42	0.23	110.0	2.33	13.96	4.00	0.29	4.62	0.33
L7	15.34	3.41	0.18	59.9	3.90	9.71	3.50	0.36	3.72	0.38
L8	6.20	1.29	0.21	18.0	2.90	2.66	1.13	0.42	1.01	0.38

Based on the results given in Table 3, it is observed that both of the probabilistic models cannot provide very satisfactory estimations of the short-term fatigue damage. From the fitting results shown in Figs. 11 and 12, significant discrepancies have been

observed in the tail region with $S \geq u+3\sigma$. Since the stress ranges in the region with $S \geq u+3\sigma$ play a dominate role in the overall fatigue damage, significant differences between the fatigue damage calculated by different methods have been found.

5. Conclusions

This paper describes probabilistic methods for the extreme ice loads prediction and fatigue damage evaluation. The ACER method has been applied for prediction of the extreme value statistics and the fatigue damage due to ice loads actions has been evaluated by application of the S-N approach. Two short-term conditions were selected in order to find some correlations between the prevailing ice conditions and the ice-induced load statistics.

By application of the ACER method, it is found that the extreme values are directly related to the number of observed ice load peaks and the distribution in the tail region. The ship-ice interaction process occurs more frequently in the bow intermediate region than the bow region for the selected ship model and the extreme ice loads in the bow intermediate region are much severer. Moreover, from a probabilistic view, severer ice condition indicates more probable to generate large ice loads. It is observed that severer ice condition corresponds to higher extreme ice loads for most of the locations in the bow and bow intermediate regions.

Probabilistic models have been applied to fit the distributions of the stress ranges. Fatigue damages evaluated by direct calculation and estimated by the probabilistic method based on the distributions of stress ranges are presented and discussed. It is found that the stress ranges in the tail region play a dominant role in the overall fatigue damage, even though the number of stress ranges in this region is very small. Moreover, the probabilistic models cannot provide satisfactory fitting results in the tail region. For these reasons, significant differences between the fatigue damages evaluated by different

methods have been observed. In addition, much severer fatigue damages have been found in the bow intermediate region as well as in the severer ice condition. These phenomenon can be explained by the fact that the fatigue damage due to ice loads actions is directly related to the number and distribution of the stress ranges, especially in the tail region.

Furthermore, the probabilistic methods described above can also be extended for long-term studies if relevant full-scale measurement data are available.

Acknowledgements

This work has been carried out within the MARTEC research project PRICE (Prediction of ice-ship-interaction for icebreaking vessels). Financial support from the Research Council of Norway (RCN, project number: 249272/O80) are acknowledged. Special thanks are given to DNV·GL for making the measurements from KV Svalbard available.

References

Bergström M, Erikstad SO, Ehlers S. 2017. The Influence of model fidelity and uncertainties in the conceptual design of Arctic maritime transport systems. Ship Technology Research.64:40-64.

Chai W, Leira BJ, Naess A. 2017. Probabilistic methods for estimation of the extreme value statistics of ship ice loads. Cold Regions Science and Technology.

Chai W, Naess A, Leira BJ, Bulian G. 2016. Efficient Monte Carlo simulation and Grim effective wave model for predicting the extreme response of a vessel rolling in random head seas. Ocean Eng.123:191-203.

Cheng Z, Madsen HA, Chai W, Gao Z, Moan T. 2017. A comparison of extreme structural responses and fatigue damage of semi-submersible type floating horizontal and vertical axis wind turbines. Renew Energy.108:207-219.

DNV. 2014. Fatigue Assessment of Ship Structures, Classification Notes No. 30.7.

Gaidai O, Storhaug G, Naess A. 2016. Extreme Value Statistics of Large Container Ship Roll. J Ship Res.60:92-100.

Guedes Soares C, Moan T. 1991. Model uncertainty in the long-term distribution of wave-induced bending moments for fatigue design of ship structures. Mar Struct.4:295-315.

Hwang M-R, Lee T-K, Kang D-H, Suh YS. A Study on Ice-induced Fatigue Life Estimation Based on Measured Data of the ARAON. Proceedings of the The 26th International Ocean and Polar Engineering Conference; 2016: International Society of Offshore and Polar Engineers.

ISSC. Arctic Technology. Proceedings of the International Ship and offshore Structures Congress (ISSC), Committee V6 report 2015 September 7th-September 10th, 2015.

Jordaan IJ, Maes MA, Brown PW, Hermans IP. 1993. Probabilistic analysis of local ice pressures. Transactions-American Scociety of Mechanical Engineers Journal of Offshore Mechnics and Arctic Engineering.115:83-83.

Karpa O, Naess A. 2013. Extreme value statistics of wind speed data by the ACER method. Journal of Wind Engineering and Industrial Aerodynamics.112:1-10.

Kotilainen M, Vanhatalo J, Suominen M, Kujala P. 2017. Predicting ice-induced load amplitudes on ship bow conditional on ice thickness and ship speed in the Baltic Sea. Cold Regions Science and Technology.135:116-126.
Kujala P, Vuorio J. 1986. Results and statistical analysis of ice load measurements on board icebreaker Sisu in winters 1979 to 1985. Winter Navigation Research Board, Helsinki, Finland.
Kujula P. 1994. On the statistics of ice loads on ship hull in the Baltic [PhD Thesis]. Helsinki University of Technology.
Leira B. 2016. Reliability updating based on monitoring of structural response parameters. Reliability Engineering & System Safety.155:212-223.
Leira B, Børsheim L, Espeland Ø, Amdahl J. 2009. Ice-load estimation for a ship hull based on continuous response monitoring. Proceedings of the Institution of Mechanical Engineers, Part M: Journal of Engineering for the Maritime Environment.223:529-540.
Lensu M. 2002. Short Term Prediction of Ice Loads Experienced by Ice Going Ships: Helsinki University of Technology.
Næss A, Gaidai O. 2009. Estimation of extreme values from sampled time series. Structural Safety.31:325-334.
Naess A, Moan T. 2012. Stochastic dynamics of marine structures Newyork: Cambridge University Press.
Nejad AR, Gao Z, Moan T. 2014. On long-term fatigue damage and reliability analysis of gears under wind loads in offshore wind turbine drivetrains. International Journal of Fatigue.61:116-128.
Nyseth H. 2006. Strain measurements on board KV Svalbard with respect to ice loading. In: Technical Report. Det Norske Veritas (DNV) Oslo, Norway.
Pfaffling A. 2007. Ship-borne sea ice thickness electromagnetic measurements. In: Technical Report.
Rahman MS, Taylor RS, Kennedy A, Ré AS, Veitch B. 2015. Probabilistic analysis of local ice loads on a lifeboat measured in full-scale field trials. Journal of Offshore Mechanics and Arctic Engineering.137:041501.
Suominen M, Kujala P. 2010. Analysis of short-term ice load measurements on board MS Kemira during the winters 1987 and 1988. Aalto University, School of Science and Technology, Espoo, Finland.
Suyuthi A, Leira B, Riska K. 2012. Short term extreme statistics of local ice loads on ship hulls. Cold Regions Science and Technology.82:130-143.
Suyuthi A, Leira B, Riska K. 2013a. Fatigue damage of ship hulls due to local ice-induced stresses. Appl Ocean Res.42:87-104.
Suyuthi A, Leira B, Riska K. 2013b. Statistics of local ice load peaks on ship hulls. Structural Safety.40:1-10.
Suyuthi A, Leira B, Riska K. 2014. A generalized probabilistic model of ice load peaks on ship hulls in broken-ice fields. Cold Regions Science and Technology.97:7-20.
Zhang S, Bridges R, Tong J. Fatigue Design Assessment of Ship Structures Induced by Ice Loading-An introduction to the ShipRight FDA ICE Procedure. Proceedings of the The Twenty-first International Offshore and Polar Engineering Conference; 2011: International Society of Offshore and Polar Engineers.